JOURNAL OF SOLID STATE CHEMISTRY **141,** 140–148 (1998)
ARTICLE NO. SC987930

Twinning in $Cs_2YbNb_6Br_{18}$ and the Atomic Structure of the Twin Interface

R. Ramlau,[1] V. Duppel, and A. Simon

Max-Planck-Institut für Festkörperforschung, Heisenbergstraße 1, 70569 Stuttgart, Germany

and

S. Cordier, C. Perrin, and M. Sergent

Laboratoire de Chimie du Solide et Inorganique Moléculaire, URA CNRS 1495, Avenue du Général Leclerc, 35042 Rennes Cedex, France

Received March 16, 1998; in revised form June 11, 1998; accepted June 16, 1998

In the search for defects in crystals of the cluster compound $Cs_2YbNb_6Br_{18}$, polysynthetic microtwinning was observed by electron diffraction and high-resolution electron microscopy (HREM), and the complete twin law could be determined. The twinning element is a twofold screw axis along [001], and the perfectly smooth twin interface is parallel to (110) of the rhombohedral unit cell. From the twin law a structure model of the twin intergrowth zone was deduced. The model assumes a fully coherent twin interface. Within the twin intergrowth zone, the Nb_6Br_{18} clusters as well as all the coordination relations between clusters, Yb atoms, and Cs atoms are preserved—and thus the chemical composition. Computer-simulated HREM images of the twin interface were generated on the basis of this model. Comparison with experimental images showed excellent agreement. Crystallographic relations between the pseudocoincidence lattices of twins are discussed, as well as the Br coordination polyhedra of interfacial Yb and Cs atoms. © 1998 Academic Press

INTRODUCTION

During our investigations on new quaternary niobium bromides $A_xRENb_6Br_{18}$ (A = alkali metal, RE = rare earth metal) with divalent rare earth metals as countercations, we have obtained two isotypical cluster compounds $Cs_2RE^{II}Nb_6Br_{18}$ (RE = Eu, Yb) which crystallize in space group $R\bar{3}$. The clusters consist of an octahedral Nb_6 core which is edge-capped by twelve inner bromines Br^i and bound to six apical, i.e., outer, bromines Br^a. The arrangement of the $Nb_6Br^i_{12}Br^a_6$ clusters, located in the center of the rhombohedral unit cell, corresponds to a fcc packing; the Cs and RE lie at $x\ x\ x$ and 0 0 0, respectively (Fig. 1). For the other rare earth metals, we have obtained a further series of cluster compounds $CsRE^{III}Nb_6Br_{18}$ which likewise crystallize in the trigonal system, but with space group $P\bar{3}1c$. The Nb_6Br_{18} clusters are centered at the origin of the unit cell and arranged in a pseudo-simple-hexagonal packing, while RE and Cs occupy the $\frac{2}{3}\ \frac{1}{3}\ \frac{1}{4}$ and $\frac{2}{3}\ \frac{1}{3}\ \frac{3}{4}$ positions, respectively (1). It seems worth mentioning that both types of compounds, $Cs_2RE^{II}Nb_6Br_{18}$ and $CsRE^{III}Nb_6Br_{18}$, exhibit an identical layer of Nb_6Br_{18} clusters parallel to the basal plane of their hexagonal unit cells (Fig. 2).

In quaternary tantalum bromides $A_xRETa_6Br_{18}$, the rare earth metals europium and ytterbium can have the $+2$ or $+3$ oxidation state, which leads, during synthesis, to mixtures of the $R\bar{3}$ and $P\bar{3}1c$ varieties when the monovalent alkali metal is cesium. On the other hand, in niobium chlorides $A_xRENb_6Cl_{18}$, europium is divalent but ytterbium is trivalent, with the respective compounds crystallizing in $R\bar{3}$ and $P\bar{3}1c$. Hence, it seems that the oxidation state of these two rare earth metals is greatly influenced by the metal–halogen system (2).

In all these compounds, the M_6 cluster core (M = Nb, Ta) is nonmagnetic, since it possesses 16 valence electrons. Consequently, we have observed only the magnetism of the rare earth ions, which was in good agreement with the theoretical value of their effective moments. However, in the case of $Cs_2YbNb_6Br_{18}$ the results of magnetic measurements gave an effective moment intermediate between those of Yb^{II} and Yb^{III}. Several possibilities have been envisaged to explain this feature and, to solve this problem definitively, we had planned to provide additional structural information by X-ray single-crystal diffraction. The poor quality of the $Cs_2YbNb_6Br_{18}$ crystals, however, prevented this structure determination. In the course of all our X-ray single-crystal studies on the $A_xRENb_6Br_{18}$ series, this was the first time that we encountered such a problem of crystallization. We

[1] To whom correspondence should be addressed. E-mail: ramlau@simix.mpi-stuttgart.mpg.de.

0022-4596/98 $25.00

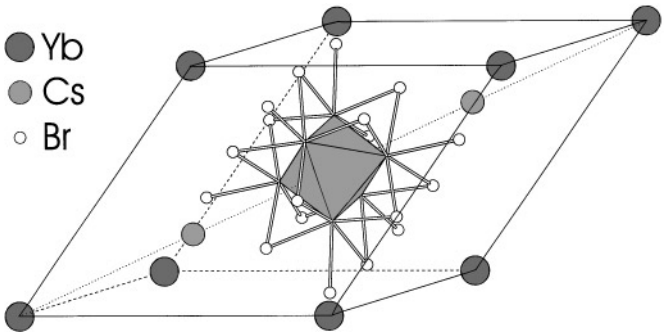

FIG. 1. Rhombohedral unit cell of the $Cs_2YbNb_6Br_{18}$ structure (space group $R\bar{3}$, $a_R = 1.0713(2)$ nm, $\alpha_R = 54.84(1)^\circ$). The octahedral Nb_6 cluster core is located at 0.5 0.5 0.5, and cesium is at 0.277 0.277 0.277 on the trigonal axis (dotted line).

assumed that this was due to chemical intergrowth of $CsYbNb_6Br_{18}$ and $Cs_2YbNb_6Br_{18}$ on a microscopic scale, which may also be described as stacking disorder of the Nb_6Br_{18} cluster layers along the trigonal axis.

High-resolution electron microscopy is an appropriate means to investigate defects on a microscopic scale, to determine their nature and, even, to obtain information on their atomic structure. It seemed therefore promising to apply this method to the compound $Cs_2YbNb_6Br_{18}$.

EXPERIMENTAL

Synthesis of $Cs_2YbNb_6Br_{18}$

The title compound was synthesized (3) by solid-state reaction from stoichiometric amounts of CsBr (Prolabo, purity 99.5%), $NbBr_5$ (Ventron, purity 99.998%), $YbBr_3$ (prepared from Yb_2O_3 according to the procedure described in (4)), and Nb (Ventron, purity m2N8). The mixture—handled under an inert atmosphere—was pressed into a pellet and heated at 750°C for 24 h in an evacuated sealed silica tube, together with some pieces of niobium foil. The hexagonal cell parameters were determined from the X-ray powder pattern with silicon as internal standard, recorded with an INEL CPS 120 diffractometer and refined by least-squares calculation: $a_H = 0.9867(1)$ nm, $c_H = 2.7218(3)$ nm (parameters of the corresponding rhombohedral unit cell: $a_R = 1.0713(2)$ nm, $\alpha_R = 54.84(1)^\circ$). The compound was obtained as a blackish-green microcrystalline powder. In the course of our electron microscopy investigations, it became obvious that the powder contained a few lath-shaped crystallites that, according to electron probe microanalysis (EPMA), proved to be CsBr.

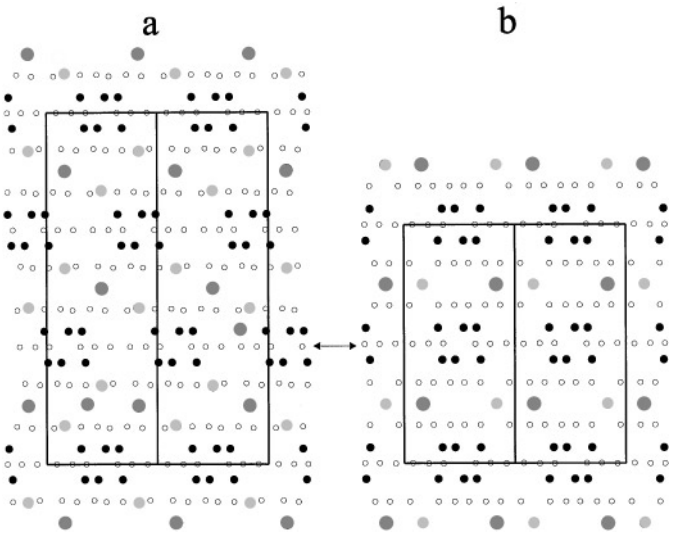

FIG. 2. Structures of (a) $Cs_2YbNb_6Br_{18}$ (space group $R\bar{3}$) and (b) $CsYbNb_6Br_{18}$ (space group $P\bar{3}1c$) in their hexagonal unit cells projected along [110]. Both structures offer an identical layer of clusters (marked). Yb, dark-gray full circles; Cs, light-gray full circles; Nb, black full circles; Br, open circles.

Electron Microscopy

A small amount of the powder was finely crushed in an agate mortar, then suspended in *n*-butanol, and fixed on a holey carbon film. High-resolution electron microscopy (HREM) and selected–area electron diffraction (SAD) investigations were performed with a Philips CM30/SuperTWIN electron microscope equipped with a LaB_6 cathode. Operating at 300 kV, the microscope has a point resolution of 0.19 nm. With the particular specimen holders used, a maximum tilt of $\pm 25^\circ$ was possible in two directions. SAD patterns were taken using a selected-area diaphragm which made the diffraction information originate from a specimen region 250 nm in diameter. Complementary EPMA by energy-dispersive X-ray spectroscopy (EDXS) was carried out using a Noran HP-Ge detector with an ultrathin window and a Voyager–I system.

The EMS program package (5) was used for the simulation of HREM images, with exit-wave functions calculated according to the multislice formalism. The spherical aberration constant C_S amounted to 1.15 mm, the defocus spread parameter was $\Delta = 7$ nm, and the illumination semiangle was determined to be $\alpha = 1.2$ mrad. The relatively high value of α is explained elsewhere (6).

HREM images and SAD patterns were partly registered on photographic material and partly with a Gatan Slow-Scan CCD Camera 694 (1024×1024 pixels). Amorphous surface layers, sometimes existing on the investigated crystal fragments, made the HREM images a little blurred, and noise reduction by Fourier filtering seemed favorable. All of the HREM images reproduced in this paper were Fourier filtered (Gatan Digital-Micrograph software) applying a band-pass mask. Much care had to be taken not to lose information on the defect structure. In the case of HREM images showing the ideal structure of $Cs_2YbNb_6Br_{18}$ (Figs. 3a–c), additionally, a periodic mask was applied.

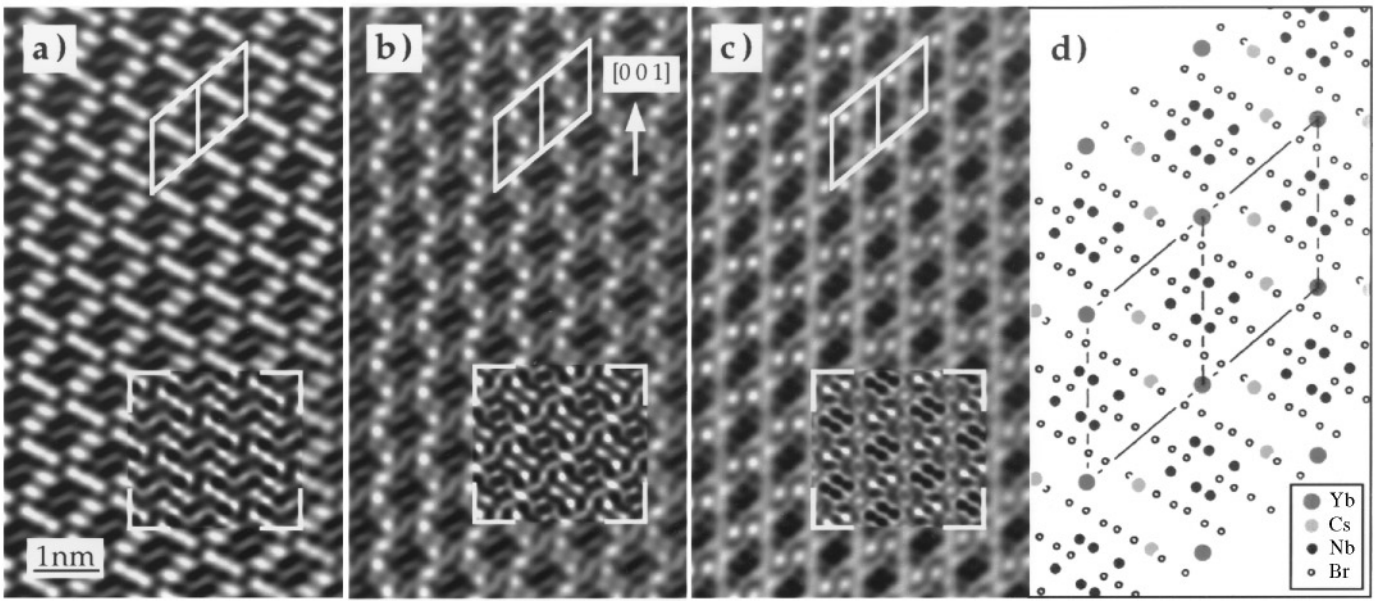

FIG. 3. (a–c) HREM images of $Cs_2YbNb_6Br_{18}$ in $[1\bar{1}0]$ orientation. Unit cell and computer-simulated images are inserted. Specimen thickness $t = 3$ nm; (a) defocus value $\Delta f = -50$ nm, (b) $\Delta f = -80$ nm, (c) $\Delta f = -110$ nm. (d) Structure of $Cs_2YbNb_6Br_{18}$ in the same projection but at an enlarged scale. By comparison of (a) with (d) it is realized that (a) is a contrast-inverted map of the atomic potential. For further explanations, see the text.

RESULTS AND DISCUSSION

Ideal Structure

Preliminary investigations showed that the $\langle 1\bar{1}0\rangle$ orientations are frequently offered by the crystal fragments and are most suitable for HREM of $Cs_2YbNb_6Br_{18}$. Indices always refer to the rhombohedral unit cell with the parameters given earlier. Figures 3a–c show a series of HREM images taken with different defocus values Δf. Computer simulations are inserted. (Since no positional parameters were available for $Cs_2YbNb_6Br_{18}$, all the data necessary for the computer simulation of images were taken from the isotypical compound $Cs_2EuNb_6Br_{18}$ (1), including the cell parameters, which deviate only slightly from those of the title compound. Nevertheless, experimental HREM images and simulated ones are in good agreement.) Because of the complexity of the investigated structure and the limited resolving power of the microscope, it is not possible to resolve every single atom. Structural units, however, can be easily identified.

Figure 3a was taken with $\Delta f = -50$ nm, which means near the Scherzer optimum defocus $\Delta f_{\text{Scherzer}} = -60$ nm. In the case of very thin specimens, when the weak-phase approximation holds, this defocus allows imaging of atoms or unresolved assemblies thereof in black, and of interspaces between atoms in white. To put it in other terms, the HREM image is then a contrast-inverted map of the atomic potential and may be interpreted straightforwardly. For further understanding, it seems worth comparing Fig. 3a with the projected crystal structure in Fig. 3d very carefully. The interrupted white lines, for example, in Fig. 3a represent the spaces between the cluster layers, with the interruptions being caused by the Yb atoms. Different features of the structure may be highlighted in other images of a defocus series (or imaging specimens of different thickness), even when the straightforward interpretation is no longer allowed. In Fig. 3c, for instance, the black double spots represent the Nb_6 cluster core.

Twinning

There is no indication for chemical intergrowth of a phase $CsYbNb_6Br_{18}$ in a matrix of $Cs_2YbNb_6Br_{18}$. The $Cs_2YbNb_6Br_{18}$ itself, however, is twinned on a submicroscopic scale. In rare cases, the twinned individuals are rather extended. More frequently, thin twin lamellae, from a few nanometers to 100 nm thick, with plane interfaces, which could be imaged edge-on in $[1\bar{1}0]$-oriented specimens, are observed (Fig. 4a). This configuration implies a certain tendency to form polysynthetically twinned structures; i.e., thin twin lamellae—one parallel to the other—occur repeatedly. Repeated twinning with the twin interfaces being not parallel to each other, which gives rise to multiply twinned particles, is less frequently observed. Figure 4c shows the SAD pattern for a defect such as that illustrated in Fig. 4a, but with a little thicker twin lamella. Both the matrix and the lamella are in an orientation of type $\langle 1\bar{1}0\rangle$. In the following, it is assumed that the matrix is $[1\bar{1}0]$ oriented.

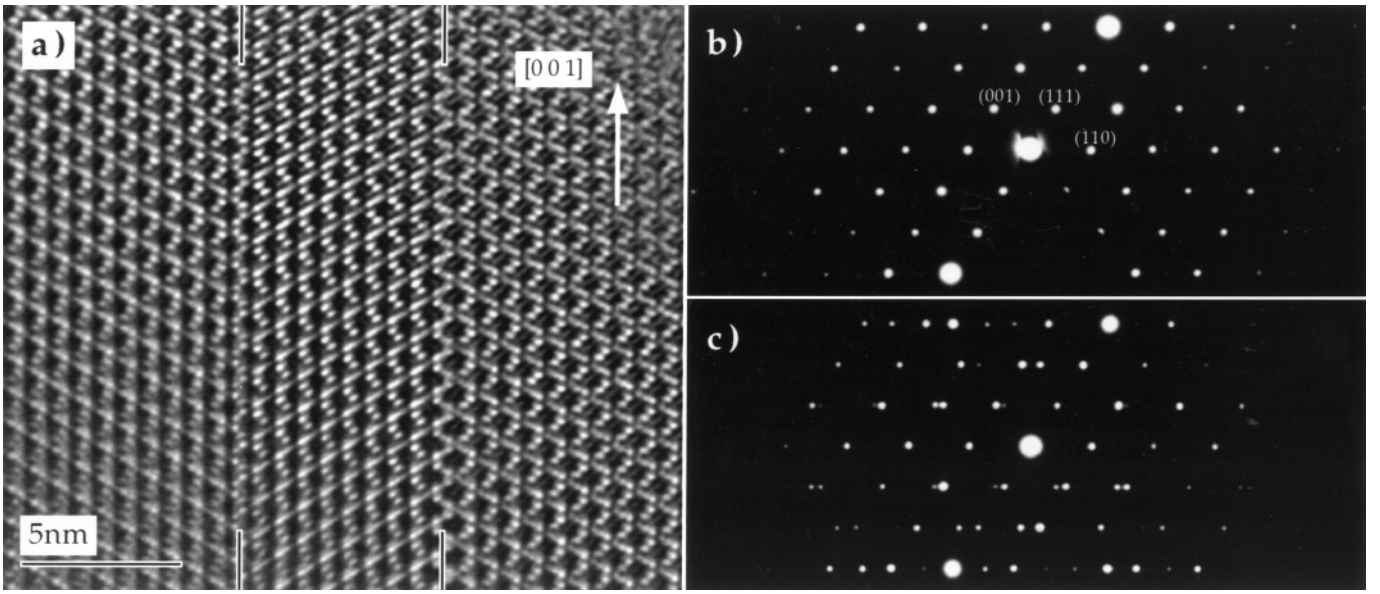

FIG. 4. (a) Twin lamella in $Cs_2YbNb_6Br_{18}$ imaged edge-on with the matrix (left and right of the marked lamella) being in $[1\bar{1}0]$ orientation. The twin interfaces are parallel to the (110) plane; the boundary lines, seen in the projection, are parallel to the [001] direction. (b) SAD pattern of the untwinned matrix in $[1\bar{1}0]$ orientation. (c) SAD pattern of a twinned region in $Cs_2YbNb_6Br_{18}$ as shown in (a).

From patterns like this and from appropriate stereographic projections of the ideal crystal structure, a number of twinning laws may be proposed: (i) reflection at the (110) plane; (ii) rotation by 180° around the [001] axis; (iii) reflection at a plane that is parallel to the $[1\bar{1}0]$ axis and orthogonal to the (110) plane (There is no such plane with low indices. However, the plane (447) could approximately act as a mirror plane ($\angle(110),(447) = 90.5°$). The fact that there is no mirror plane that exactly fulfils the condition of orthogonality to (110) may also be deduced from the SAD pattern given in Fig. 4b); (iv) rotation by 180° around an axis that is orthogonal to the $[1\bar{1}0]$ axis and orthogonal to the (110) plane (There is no such axis with low indices. However, the axis $[13,13,\overline{15}]$ could act as an axis of rotation ($\angle(110), [13,13,\overline{15}] = 90.0°$).).

The twinning laws i and ii should be preferred because of their simplicity. Moreover, it becomes immediately evident from Fig. 4a that the intergrowth planes of the twins are parallel to (110). If twinning law i is valid, then the mirror plane and the intergrowth plane would be identical. If twinning law ii is valid, then the rotation axis would lie in the intergrowth plane. All geometrical details in Fig. 4a, which means distances of and angles between lattice planes, are in accordance with both law i and law ii. Let the first individual be in $[1\bar{1}0]$ orientation. If law i is acting, the second individual will again be brought into $[1\bar{1}0]$ orientation. By action of law ii it will be brought into $[\bar{1}10]$ orientation. Since HREM images are projections by nature, the two possibilities cannot be distinguished. This will, however, be possible by tilting the specimen into a different orientation. In Fig. 5 the matrix orientation is tilted exactly by 19.9° around the normal to the interface plane, from $[1\bar{1}0]$ into $[3\bar{3}\bar{1}]$. This operation allows one to view the twin lamella edge-on again. With law i acting, the twin lamella would now be in $[3\bar{3}\bar{1}]$ orientation; with law ii, in $[\bar{3}3\bar{1}]$

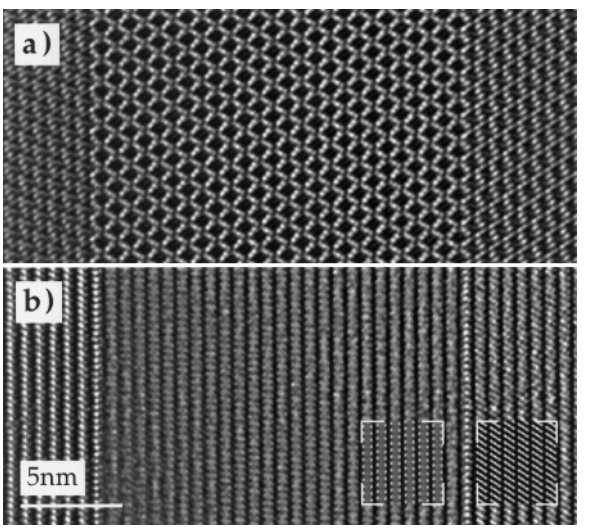

FIG. 5. HREM images of an edge-on twin lamella in $Cs_2YbNb_6Br_{18}$: (a) matrix in $[1\bar{1}0]$ orientation and lamella in $[\bar{1}10]$; (b) matrix tilted into $[3\bar{3}\bar{1}]$ orientation with lamella then being in $[\bar{3}3\bar{1}]$ orientation. Computer-simulated images are inserted in (b); $t = 6.3$ nm, $\Delta f = -60$ nm.

orientation. Inspection of the corresponding SAD pattern is not helpful, because dynamical diffraction effects prevent an unambiguous interpretation. However, comparing the HREM image (taken from thinner parts of the specimen) with simulated images for the two considered crystal orientations, $[3\bar{3}\bar{1}]$ or $[\bar{3}3\bar{1}]$, is in favor of the validity of law ii. This result will also be confirmed by structural considerations in a later paragraph. Nevertheless, it remains an open question whether the twinning element contains a translational component and at which crystallographic positions the twinning element as well as the intergrowth plane are located. Both questions cannot be answered on the basis of SAD patterns but by careful inspection of the HREM micrographs.

Structure of the Twin Interface

Figure 6 shows the twin-interface region in an enlarged HREM micrograph. Projections of the crystal structure are inserted at their exact positions on both sides of the twin interface. It becomes immediately obvious that the twin interface does not involve the Yb atoms of the ideal structure and, consequently, does not cross the Nb_6Br_{18} clusters, which is a quite reasonable result with regard to chemical bonding. The clusters themselves do not possess a twofold axis along [001]. On the other hand, they are too rigid (at least the core and the 12 Br^i atoms) to be modified in the twin interface. Instead of involving the cluster cores and, consequently, the Yb positions at the corners of the unit cell, the twin interface comprises the point 0.5 0 0, which means the interface touches the Cs atoms at 0.277 0.277 0.277. Moreover, it is clear from Fig. 6 that the twinning law established earlier must be modified. Besides the 180° rotation around the [001] axis, there is a translation by $\frac{1}{2}$ [001]; i.e., the twinning element is a twofold screw axis.

To visualize the intergrowth zone of the twins more directly, a ball-and-stick model of the structure was built. With this model, it was easy to realize that the two twin individuals must additionally be shifted against one another along the $[1\bar{1}0]$ axis. This shift could not be observed in the HREM micrograph of Fig. 6 because it is along the projection direction. Until now, we only placed the twinning axis in a (110) plane which intersects point 0.5 0 0, and one degree of freedom is left for its exact location. With the twofold [001] screw axis also placed at point 0.5 0 0, the relative shift of the twin individuals along $[1\bar{1}0]$ is, however, also taken into account correctly. Figure 7 illustrates the situation schematically. The immediate vicinity on both sides of the twin interface; i.e., the twin intergrowth zone, is shown in a projection along $[13,13,\overline{15}]$.

The second twin individual fits to the first like a key into its lock. In the intergrowth zone every Cs atom is coordinated by 4 clusters, every cluster by 8 Cs atoms, and every Yb atom by 6 clusters—just as in the ideal structure. If one regards the Nb_6Br_{18} clusters as rigid spheres, almost no change will be discernible. The Yb atoms and the clusters are forming pseudocoincidence lattices that extend from one

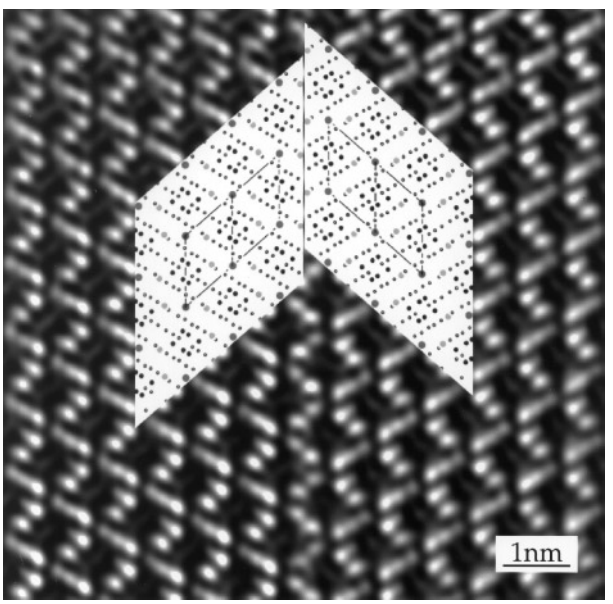

FIG. 6. Enlarged HREM image in $\langle 1\bar{1}0\rangle$ orientation with the twin interface parallel to (110). On both sides of the interface, representations of the projected structures (cf. Fig. 3d) are inserted.

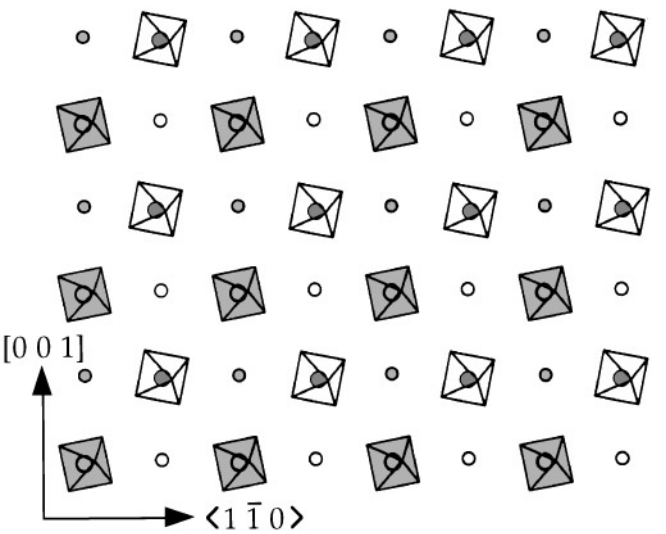

FIG. 7. Representation of the twin intergrowth zone in a projection along $[13,13,\overline{15}]$ (indexing with respect to one twin individual). The model is based on the twinning element being a twofold screw axis along [001] placed at point 0.5 0 0 of the rhombohedral unit cell. The twin interface is seen in plan view; open symbols refer to the slice below the interface, and shaded symbols to the slice above. Nb_6 cluster cores, octahedra; Yb, large circles (in front or behind the octahedra); Cs, smaller circles (between the octahedra); Br omitted for the sake of clarity.

twin individual to the other (Fig. 8a). In particular, there will be no changes in the "sphere" packing of clusters.

This astonishing feature becomes understandable when we consider the particular characteristics of the $Cs_2YbNb_6Br_{18}$ structure: It is possible to choose a larger rhombohedral unit cell for this structure, with parameters $a^l = 1.523$ nm and $\alpha^l = 85.2^\circ$. The basic translations are now $\vec{a}^l = \vec{a} - \vec{b} + \vec{c}$, cyclicly permuted. Consequently, the lattice is pseudo fcc with α^l equal to 85.2° instead of 90°. The whole structure may be treated as built from four pseudo fcc sublattices, all interpenetrating: the Yb sublattice, the cluster sublattice, and two Cs sublattices. The twinning element formulated for the pseudo fcc Yb sublattice is a 180° rotation around $[101]^l$ at point 0.25 0.25 0 of the pseudo fcc unit cell and a translation by $\frac{1}{4}$ $[101]^l$. For an angle α^l equal to 90°, which corresponds to $\alpha_R = 60^\circ$ for the standard rhombohedral unit cell, the Yb sublattice transforms into itself by this operation. Furthermore, the cluster sublattice, with the clusters taken as rigid spheres, also transforms into itself (Fig. 8b). Eventually the two Cs sublattices transform one into the other, under the additional assumption that Cs is placed at 0.25 0.25 0.25 of the rhombohedral unit cell instead of 0.277 0.277 0.277 (Fig. 8c).

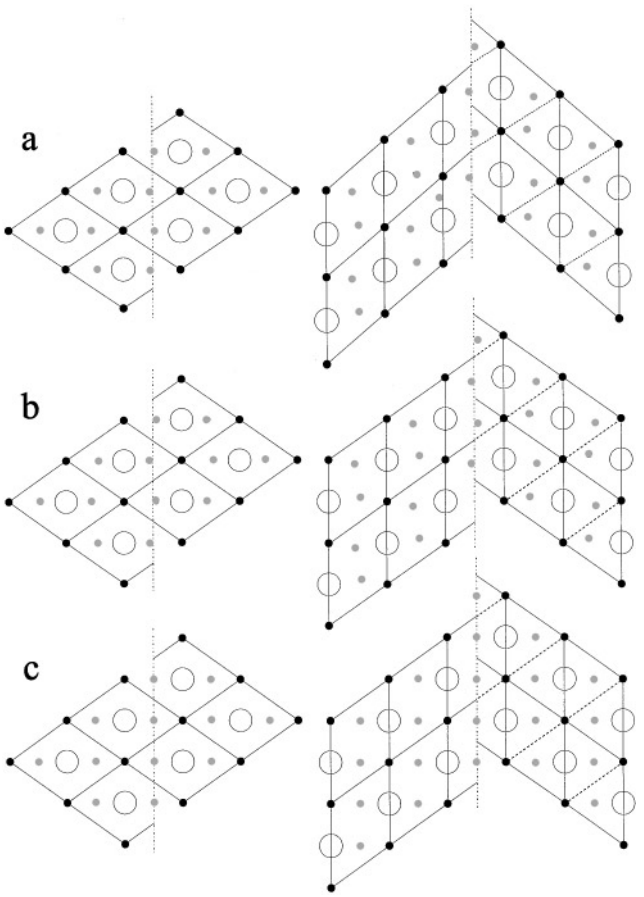

FIG. 8. Crystallographic relations between twins in [001] (left) and $\langle 1\bar{1}0 \rangle$ projection (right). The twin interface is indicated by a dot–dash line, clusters as large open circles, Yb as dark-gray full circles, and Cs as light-gray full circles. (a) Clusters idealized as of spherical symmetry: clusters and Yb atoms are forming pseudocoincidence lattices. (b) Rhombohedral angle α idealized as equal to 60° instead of 54.84°: clusters and Yb atoms are forming coincidence lattices. (c) Cs positions idealized as 0.25 0.25 0.25 instead of 0.277 0.277 0.277: clusters, Yb, and Cs atoms are forming coincidence lattices.

In summary, the $Cs_2YbNb_6Br_{18}$ structure can only twin since it deviates slightly from four interpenetrating fcc sublattices with origins at 0 0 0, 0.25 0.25 0.25, 0.5 0.5 0.5, and 0.75 0.75 0.75 and, last but not least, since the clusters are not at all spheres. With the clusters idealized as spheres, but all other features taken from the real $Cs_2YbNb_6Br_{18}$ structure, twinning would also be possible. The corresponding HREM images, however, would only display slight kinks of the lattice planes (cf. Fig. 8a) The rather drastic effects seen in the experimental HREM images originate mainly from the different orientations of the Nb_6Br_{18} clusters in the two twin individuals.

To simulate HREM images of the intergrowth zone directly, a supercell ($a^s = 2.1581$ nm, $b^s = 3.5051$ nm, $c^s = 0.9915$ nm, $\alpha^s = 90^\circ$, $\beta^s = 90^\circ$, $\gamma^s = 90^\circ$) was created, which is based on the following model: A twofold screw axis oriented along [001] is acting at point 0.5 0 0 of the rhombohedral unit cell. The Cs atoms within the intergrowth zone are still coordinated by four clusters, two belonging to one twin individual and two to the other. Consequently the threefold axes of the four coordinated clusters are no longer parallel. A Cs atom is still bound to twelve Br atoms, six belonging to each twin individual. The Yb atoms within the intergrowth zone are still coordinated by six clusters, five belonging to one twin individual and one to the other. They are still bound to six Br atoms, five of them belonging to one twin individual and one to the other. For every Nb_6Br_{18} cluster in the intergrowth zone, one Br^a atom projects into the other twin individual, where it is part of the coordination octahedron around an Yb atom. The coordinates of the 260 atoms in the supercell are given elsewhere.[2] Figure 9 shows the model-based coordination spheres for Yb and Cs in the intergrowth zone, in comparison with the respective coordination spheres in the ideal $Cs_2YbNb_6Br_{18}$ structure.

The HREM images in Figs. 10a–c show the twin intergrowth zone in a very thin specimen together with images which have been computer simulated on the basis of the model described earlier. A [001] projection of the supercell,

[2] See NAPS document No. 05478 for 8 pages of supplementary material. This is not a multi-article document. Order from NAPS c/o Microfiche Publications, 248 Hempstead Turnpike, West Hempstead, New York 11552. Remit in advance in U.S. funds only $15.00 for photocopies or $5.00 for microfiche. There is a $25.00 invoicing charge on all orders filled before payment. Outside U.S. and Canada add postage of $4.50 for the first 20 pages and $1.00 for each 10 pages of material thereafter, or $5.00 for the first microfiche and $1.00 for each microfiche thereafter.

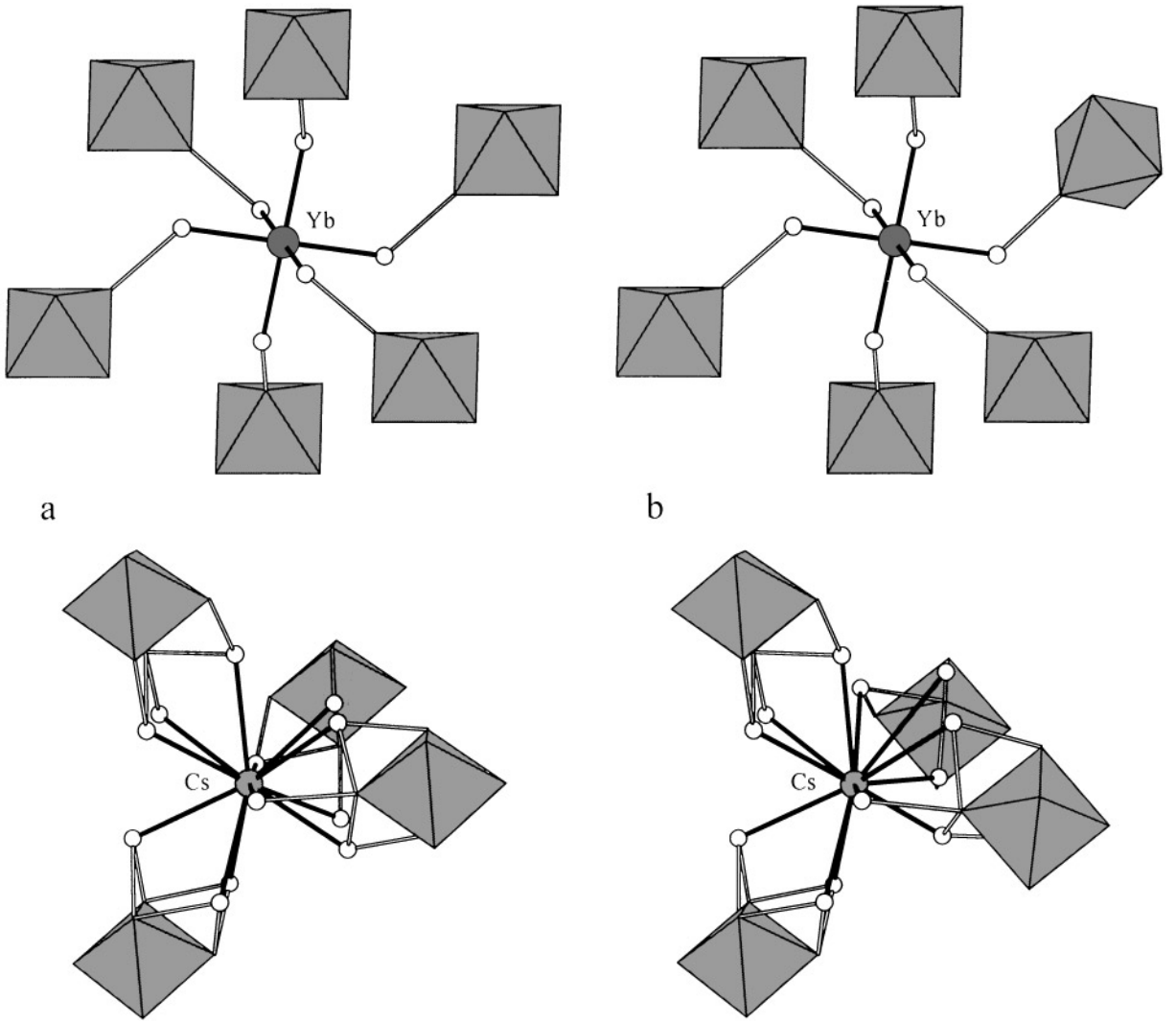

FIG. 9. Coordination spheres (a) of the Yb and Cs atoms in the ideal $Cs_2YbNb_6Br_{18}$ structure (left) and (b) of interfacial Yb and Cs atoms (right). In (b), the upper right cluster of the Yb coordination sphere and the two right clusters of the Cs coordination sphere belong to the other twin individual. Nb_6 cluster cores, shaded octahedra; Yb, dark-gray full circles; Cs, light-gray full circles; Br, open circles.

which corresponds to a rhombohedral $\langle 1\bar{1}0 \rangle$ projection, is given in Fig. 10d. When compared visually, accordance between experimental and simulated images seems excellent. If at all, a further refinement of the model structure would only be possible by quantitative methods of comparison between experimental and simulated images (7). It will be the subject of a future study to check this option.

Chemistry of the Twin Interface

It can be deduced from Fig. 9 that the coordinations of the Yb atoms in the ideal structure and in the twin intergrowth zone do not significantly deviate from one another. Consequently, there is no indication for the presence of trivalent Yb in the twin intergrowth zone. It may be speculated that a change in the Yb oxidation state could be due to one vacant Br position in the octahedral coordination of interfacial Yb atoms. The missing Br atom could then be that Br^a which belongs to a cluster in the other twin individual. There is, however, no experimental evidence in the HREM images for such vacancies occurring regularly. The fact that the ideal $Cs_2YbNb_6Br_{18}$ structure itself, as complex it may be, allows the formation of a completely coherent twin interface is not in favor of hypothetical vacancies, either. With a mirror plane as the twinning element—a possibility which has been discussed and rejected earlier—the situation would be completely different. Distortions in the intergrowth zone would be much greater, and the coordinations of Yb and Cs atoms could differ from

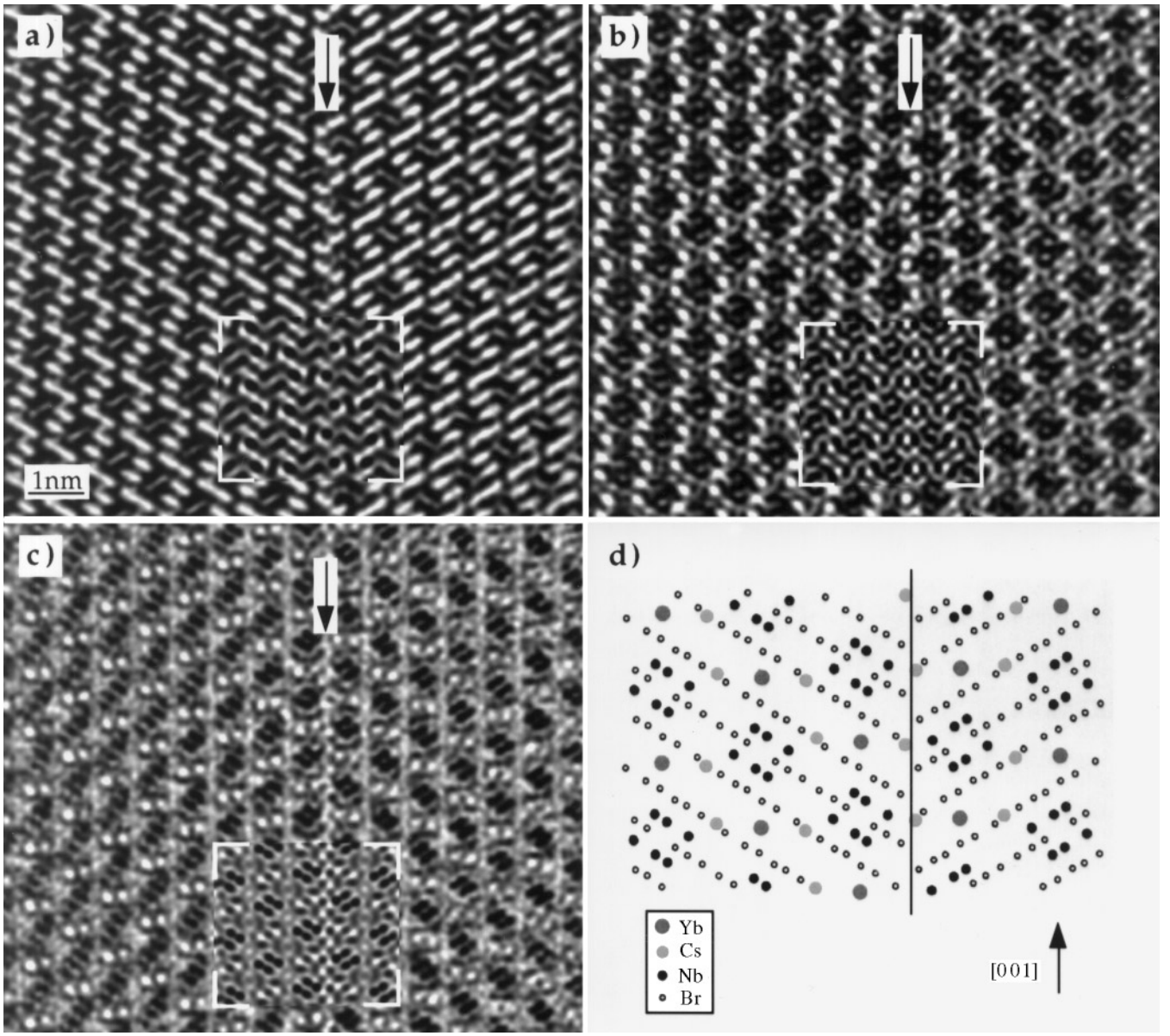

FIG. 10. HREM images of the twin intergrowth zone in $\langle 1\bar{1}0 \rangle$ orientation with the interface indicated by arrows. Computer-simulated images based on the structure model are inserted; $t = 3$ nm; (a) $\Delta f = -50$ nm, (b) $\Delta f = -80$ nm, (c) $\Delta f = -110$ nm. In (d), the complete supercell with its 260 atoms is shown in the analog projection, with the twin interface marked by a line and the rhombohedral [001] direction indicated.

those in the ideal structure. In summary, the results of HREM indicate that the chemical composition of the twin intergrowth zone is exactly that of the ideal structure. The existence of trivalent Yb in the investigated material, as postulated on the basis of magnetic measurements, is definitely not related to the twinning described herein.

Figure 9 also shows that the tetrakaidecahedral coordination of the Cs atoms in the twin intergrowth zone deviates only slightly from that in the ideal structure, but the four tripods of the coordination polyhedron are regrouped among the 12 Cs–Br bonds. As in the ideal structure, the Cs is bound to one, privileged cluster via three Br^i-type atoms and to the three other clusters via two Br^i- and one Br^a-type atoms. The threefold axis of the coordination polyhedron is no longer parallel to the threefold axis of the privileged cluster, but inclined. Virtually, the threefold axis of the coordination polyhedron is now lost because of small distortions in the bond angles and small changes in the bond lengths. It is just the high adaptability of the Cs^+ ion that allows the twin interface to be completely coherent. In

a broader sense, it is also the reason for the ready formation of microtwins, and thus for the insufficient crystallization of the compound.

As already mentioned, X-ray single-crystal analysis failed and atomic coordinates for $Cs_2YbNb_6Br_{18}$ are still missing. Data were taken from the isostructural compound $Cs_2EuNb_6Br_{18}$. Therefore, we dispensed with a quantitative discussion of bond angles and bond lengths in the coordination spheres of interfacial Yb and Cs atoms in comparison with the ideal structure. Attempts are currently being made to determine accurate atomic coordinates for $Cs_2YbNb_6Br_{18}$ from X-ray powder data by the Rietveld method (8).

CONCLUSIONS

The structural features of $Cs_2YbNb_6Br_{18}$ facilitate the formation of rotation twins during crystal growth by solid-state reaction, with the twin element being a twofold screw axis along [001]. The twin interface is completely coherent, perfectly smooth with respect to building units (not atoms!), and parallel to the (110) lattice plane. Within the twin intergrowth zone, the structure of the Nb_6Br_{18} clusters is not altered, and all clusters are coordinated by Yb and Cs atoms (and vice versa) as they are in the ideal structure. Ytterbium is bound to six Br atoms, and the octahedral coordination is identical with that in the ideal structure. Cesium is bound to twelve Br atoms but its tetrakaidecahedral coordination polyhedron is slightly modified in both bond angles and bond lengths. Polysynthetic microtwinning occurs very frequently and hinders the formation of crystals suitable for X-ray single-crystal analysis. The results of magnetic measurements having indicated an effective moment between those of Yb^{II} and Yb^{III} remain unexplained. The mixed valency of Yb is obviously not related to the twin formation. In addition, there is no evidence that phases containing Yb^{III}, as, e.g., $CsYbNb_6Br_{18}$, are chemically intergrown with $Cs_2YbNb_6Br_{18}$.

ACKNOWLEDGMENTS

R.R. is grateful to Dr. J. Köhler and Dr. U. Steinbrenner for valuable discussions.

REFERENCES

1. S. Cordier, C. Perrin, and M. Sergent, *Z. Anorg. Allg. Chem.* **619,** 621 (1993).
2. C. Perrin, S. Cordier, S. Ihmaïne, and M. Sergent, *J. Alloys Compd.* **229,** 123 (1995).
3. S. Cordier, Thesis, Université de Rennes I, 1996.
4. G. Meyer and P. Ax, *Mater. Res. Bull.* **17,** 1447 (1982).
5. P. A. Stadelmann, *Ultramicroscopy* **21,** 131 (1987).
6. R. Ramlau, *J. Solid State Chem.* **130,** 290 (1997).
7. G. Möbus, *Ultramicroscopy* **65,** 205 (1996).
8. J. Köhler, R. Ramlau, and C. Perrin, in preparation.